Title	Generalized Coupled-Line All-Pass Phasers
Author(s)	Gupta, S; Zhang, Q; Zou, L; Jiang, L; Caloz, C
Citation	IEEE Transactions on Microwave Theory and Techniques, 2015, v. 63, p. 1007-1018
Issued Date	2015
URL	http://hdl.handle.net/10722/216970
Rights	Creative Commons: Attribution 3.0 Hong Kong License

Generalized Coupled-Line All-Pass Phasers

Shulabh Gupta, *Member, IEEE*, Qingfeng Zhang, *Member, IEEE*, Lianfeng Zou, *Student Member, IEEE*,
Li Jun Jiang, *Senior Member, IEEE*, and Christophe Caloz, *Fellow, IEEE*

Abstract—Generalized coupled-line all-pass phasers, based on cascaded C-sections (CCSs), cascaded coupled-lines (CCLs), and hybrid-cascaded (HC) coupled transmission-line sections, are presented and demonstrated using analytical, full-wave, and experimental results. It is shown that for N commensurate coupled-line sections, CCL and HC phasers exhibit N group-delay peaks per coupled-line section harmonic frequency band, in contrast to the CCS configuration, which exhibits only one peak within this band. It is also shown that for a given maximum achievable coupling-coefficient, the HC configuration provides the largest group-delay swing. A wave-interference analysis is finally applied to the various coupled-line phasers, explaining their unique group-delay characteristics based on physical wave-propagation mechanisms.

Index Terms—All-pass networks, C-sections, dispersion engineering, D-sections, group-delay engineering, phasers, radio-analog signal processing (R-ASP).

I. INTRODUCTION

RADIO-ANALOG signal processing (R-ASP) has recently emerged as a new paradigm for monitoring, manipulating, and processing radio signals in real time [1]–[3]. Compared to conventional digital signal processing (DSP) techniques, R-ASP operates on signals directly in their pristine analog form to execute specific operations enabling microwave or millimeter-wave and terahertz applications. It thus provides a potential solution, especially at high frequencies, to overcome the drawbacks of DSP techniques, which include high-cost A/D and D/A conversion, high power consumption, low speed, and high complexity.

The heart of an R-ASP system is a phaser (refer to Section V-A for a detailed discussion on phaser terminology), which is a component exhibiting a specified frequency-dependent group-delay response within a given frequency range [1]. When a broadband signal propagates through a phaser, its

spectral components progressively separate from one another in the time domain due to their different group velocities, a well-known phenomenon commonly referred to as chirping. This spectral discrimination in the time domain allows manipulating spectral bands individually and directly in the time domain, thereby enabling several high-speed and broadband processing operations. Some recently demonstrated R-ASP applications include signal receivers and transmitters for communications [4], [5], frequency meters and discriminators for cognitive networks [6], [7], spectrum analyzers for instrumentation [8]–[10], signal manipulation for efficient signal processing [11], [12] and chipless tags for RF identification (RFID) systems [13].

Phasers can be either of reflective type or transmission type. Reflective-type phasers are single-port structures, which are converted into two-port structures using a broadband circulator or a hybrid coupler. They are mostly based on the principle of Bragg reflections, and include microstrip chirped delay lines [14], artificial dielectric-substrate-based phasers [15] and reflection-type waveguide phasers [16]. While reflection-type phasers impose less constraints on the design parameters of the phaser compared to transmission-type phasers [17], their requirement of an external one-port to two-port conversion component, incurring additional loss along with undesired phase distortions in the overall delay response, is a major drawback. Transmission-type phasers, on the other hand, are inherently two-port components. Surface acoustic wave (SAW) devices [18], and magneto-static devices [19] are some classical representatives of these phasers, but they are suitable only for very low frequencies and narrow-bandwidth applications. While some recently proposed transmission-type phasers, based on coupled-matrix analysis, offer great synthesis flexibility for advanced group-delay engineering, they are usually restricted to narrowband designs [20], [21]. For broader band applications, coupled-line all-pass phasers are more suitable, also offering greater design simplicity and benefiting from efficient synthesis procedures [22]–[25].

The coupled-line all-pass phasers reported to date are based on cascaded C-sections (CCSs) and/or D-sections synthesizing prescribed group-delay responses [25], [26]. On the other hand, a *longitudinal cascade* of commensurate coupled transmission lines was first demonstrated in [22]. In this work, a third type of cascading configuration is proposed based on a combination of a CCS and a cascaded couple-line (CCL) configuration, hereby termed the hybrid cascade (HC). The corresponding coupled-line phaser is called an HC coupled-line phaser. The HC coupled-line phaser was first introduced in [27] and later used in group-delay engineering in [28]. This set of three cascading configurations, CCL, CCS, and HC, represent the fundamental cascading schemes upon which more complex phasers
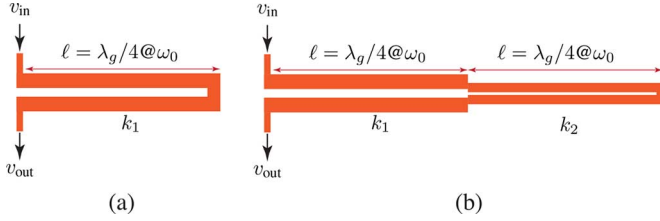
Fig. 1. Transmission-type all-pass phaser topologies. (a) C-section and (b) D-section with ω_0 being the quarter-wavelength frequency of a transmission line.

can be constructed, leading to vast variety of coupled-line all-pass phasers with rich and exotic dispersion characteristics. Further, the group-delay characteristics of these three cascaded configurations are investigated and compared in details and their unique properties are explained using a rigorous wave-interference analysis.

This paper is organized as follows. Section II introduces the CCS, CCL, and HC coupled-line phaser topologies with a comparison of their group-delay characteristics based on their analytical transfer functions. It also presents corresponding fabricated prototypes along with measured results, validating the analytical models and confirming the various group-delay characteristics. Section III presents the wave-interference mechanisms that may be used to construct a general transfer function with coupled-line all-pass phasers. These mechanisms are then used to explain some unique group-delay features of CCL and HC coupled-line phasers. Finally, Section IV provides conclusions.

II. COUPLED-LINE ALL-PASS PHASERS

A. Basic Transfer Functions

All-pass transfer functions are based on two building-block transfer functions, the C-section and the D-section transfer functions [29].

A C-section transfer function can be realized by a two-port transmission-line structure, consisting of a (four-port) coupled-line coupler with its through and isolated ports interconnected by an ideal transmission-line section, as shown in Fig. 1(a). Its transfer function can be derived by applying the interconnection boundary condition between the ingoing and outgoing waves at the two end ports of the coupler. The C-section transfer function is given by

$$S_{21}(\theta) = \left(\frac{\rho - j \tan \theta}{\rho + j \tan \theta} \right) \qquad (1a)$$

with

$$\rho = \sqrt{\frac{1+k}{1-k}} \qquad (1b)$$

where k is the coupling coefficient between the coupled-lines forming the structure. Its all-pass nature, $|S_{21}| = 1, \forall \theta$, is immediately verified by noting that the magnitudes of the numerator and denominator in (1a) are equal, and it may also be verified that the function provides a frequency-dependent group-delay response reaching a maximum value at $\theta = (2m - 1)\pi/2$, where m is an integer. This condition corresponds to frequencies where the length of the coupled-line section is an odd multiple of a quarter-wavelength. Upon the high-pass to low-pass transformation $s = j \tan \theta$, the C-section is seen to be

a first-order phaser, with one real pole and one real zero, placed symmetrically about the imaginary axis in the s-plane.

The derivation of a generalized transfer function corresponding to a coupled-line coupler terminated with an arbitrary all-pass load with transfer function S_0 is provided in the Appendix, Section B and reads

$$S_{21}(\theta) = b + \frac{a^2 S_0}{1 - b S_0} \qquad (2)$$

where, in (2), a and b are the through and coupled transfer functions of the coupler without the end connection. The C-section transfer function is a particular case of this network with $S_0 = 1$.

The second-order transmission-line all-pass phaser is the D-section, which consists of a coupled-line coupler terminated with a C-section, as shown in Fig. 1(b). Using the general transfer function form (2) with S_0 given by (1a), the transfer function of a D-section is found as

$$S_{21}(\theta) = \left(\frac{1 - \rho_a \tan^2 \theta - j \rho_b \tan \theta}{1 - \rho_a \tan^2 \theta + j \rho_b \tan \theta} \right) \qquad (3a)$$

with

$$\rho_a = \sqrt{\frac{1 - k_1}{1 + k_2}} \sqrt{\frac{1 + k_1}{1 - k_2}} \qquad (3b)$$

and

$$\rho_b = \sqrt{\frac{1 - k_1}{1 + k_1}} + \sqrt{\frac{1 - k_2}{1 + k_2}} \qquad (3c)$$

where $k_{1,2}$ are the coupling coefficients of the two sections. Upon the transformation $s = j \tan \theta$, the D-section is seen to be a second-order phaser, with two pairs of complex para-conjugate zeros and poles in the s-plane.

B. Phaser Topologies

The group-delay profiles of a C-section and a D-section have a specific and restricted shape that depend on the length and coupling coefficients of the sections involved. However, combining several coupled-line sections in an appropriate fashion allows synthesizing virtually arbitrary prescribed group-delay responses between the input and the output ports within a given frequency range. Such phasers can be conceptualized and categorized based on how the different coupled-line sections are connected together. The three basic configurations shown in Fig. 2 are possible and are described below.

1) *CCS phaser.* In this configuration, several C-sections are cascaded in the direction that is transverse to the axis of the transmission lines forming the C-sections, as shown in Fig. 2(a). The corresponding transfer function is then simply the product of the individual C-section transfer functions, and thus reads

$$S_{21}^{\text{CCS}}(\theta) = \prod_{i=1}^{N} \left(\frac{\rho_i - j \tan \theta}{\rho_i + j \tan \theta} \right) \qquad (4)$$

where $\rho_i = \sqrt{(1 + k_i)/(1 - k_i)}$, k_i being the coupling coefficient of the ith section.

2) *CCL phaser.* In this configuration, several coupled-line sections are cascaded in the direction of the transmission lines forming the coupled-lines, as shown in Fig. 2(a),
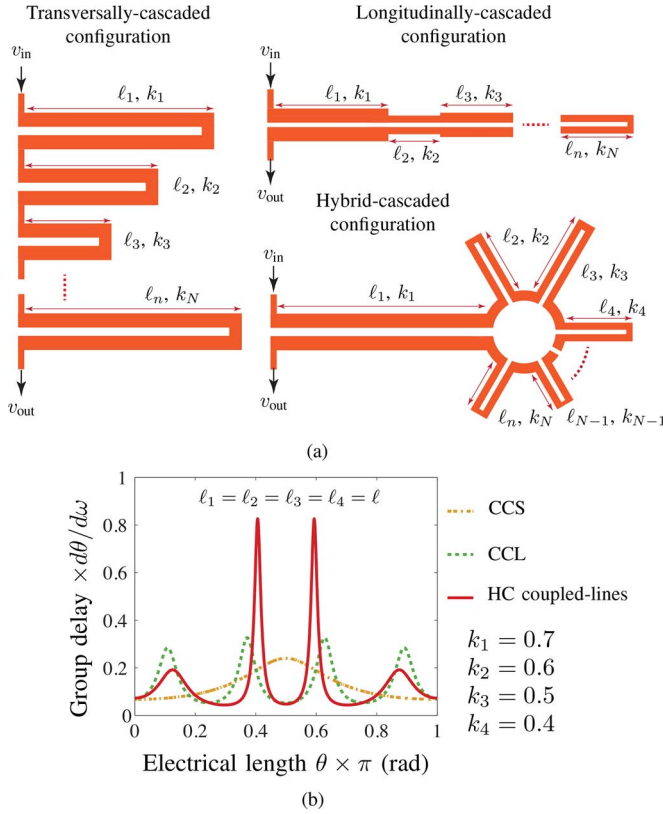
Fig. 2. Cascaded coupled-line all-pass phasers. (a) Generic topologies for a CCS, CCL, and HC coupled-line phasers. (b) Typical group-delay response of the three phaser topologies in (a) over the lowest coupled-line section harmonic frequency band with $N = 4$ coupled-line sections of identical length $\ell_i = \ell$.
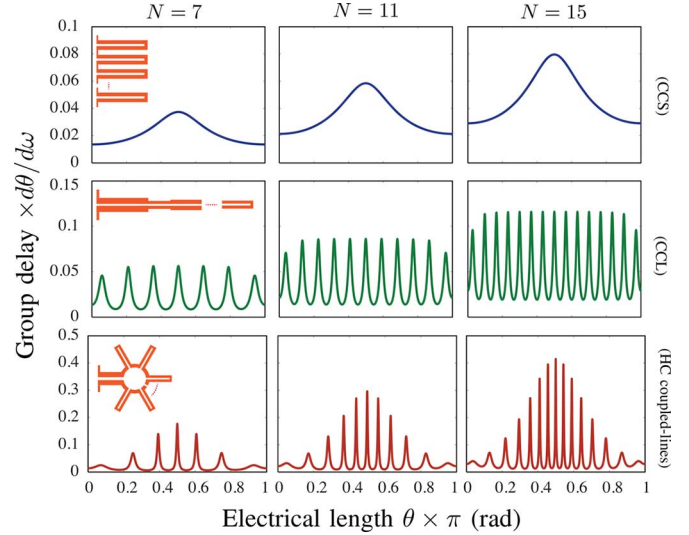

Fig. 3. Typical group-delay responses for the different cascaded coupled-line phasers in Fig. 2(a) with different numbers N of coupled-line sections of length. Here, all the phaser sections have the same length ℓ, while $k_1 > k_2 > k_3 \ldots > k_N$.

of simplicity and comparability, we shall restrict our analysis to the case of commensurate coupled-line sections (i.e., coupled-line sections having all the same length). However, it should be kept in mind that the above analytical transfer functions are general and that the corresponding phasers exhibit much richer synthesis possibilities than those presented below.

C. Group-Delay Response

The three configurations in Fig. 2(a) exhibit very different group-delay responses, as shown in Fig. 2(b) for the case of $N = 4$ and $\ell_1 = \ell_2 = \ell_3 = \ell_4 = \ell$. Under the latter condition, the CCS phaser has a delay shape similar to that of a regular C-section, with a single delay maximum over the lowest coupled-line section harmonic frequency band, $\theta \in [0, \pi]$. In contrast, the CCL configuration exhibits four delay peaks within the same bandwidth. These peaks are quasi-uniformly spaced and quasi-equal in magnitude, with group-delay swings, $\Delta\tau = \tau_{\max} - \tau_{\min}$, that are larger than those obtained in the CCS case.[1] Similar to the CCL case, the HC coupled-line phaser exhibits four delay peaks, but with dramatically different characteristics. While the outermost delay peaks are lower, the center ones have a steep slope within a narrow bandwidth and thus exhibit a very large delay swing $\Delta\tau$. Moreover, it is observed that the two central peaks are closer to the each other compared to the CCL case. Thus, for a given maximum achievable coupling k, the HC coupled-line phaser provides the largest group delay swing $\Delta\tau$ among the three configurations.

Fig. 3 shows the typical group-delay responses of these three configurations for different number of coupled-line sections N. While the CCS phaser maintains a single delay peak across the bandwidth for all Ns, the number of delay peaks in the CCL and the HC case scales with N. In general, for N coupled-line sections, the group delay exhibits N delay peaks within a periodic band. The trends observed in Fig. 2(b) are confirmed as follows.

with the last section being a C-section [30]. The corresponding transfer function can be derived by iteratively constructing the load transfer functions starting from the last coupled-line section towards the input port, as derived in Appendix, Section C. The result is

$$S_{21}^{\mathrm{CCL}}(\theta) = S_1(\theta) = b_1 + \frac{a_1^2 S_2(\theta)}{1 - b_1 S_2(\theta)} \tag{5}$$

where $S_2(\theta)$ is the overall transfer function of the structure starting from the second to the Nth coupled-line section. It is to be noted that a D-section is the particular case of an CCL coupled-line phaser with $N = 2$.

3) *HC coupled-line phaser.* This configuration consists of a combination of CCS and CCL coupled-line sections, as illustrated in Fig. 2(c). This may be seen as a coupled-line coupler terminated with a CCS phaser. The corresponding transfer function can be written using the CCS transfer function as S_0 in (2), leading to

$$S_{21}^{\mathrm{HC}}(\theta) = b_1 + \frac{a_1^2 S_0(\theta)}{1 - b_1 S_0(\theta)} \tag{6a}$$

$$S_0(\theta) = \prod_{i=2}^{N} \left(\frac{\rho_i - j \tan\theta}{\rho_i + j \tan\theta} \right). \tag{6b}$$

The diversity of possible transfer functions provided by the CCS, CCL, and HC coupled-line phasers for general parameters is too great to be tractable in such a paper. Therefore, for the sake

---

[1]Note that the response can be drastically different in the case of noncommensurate sections.
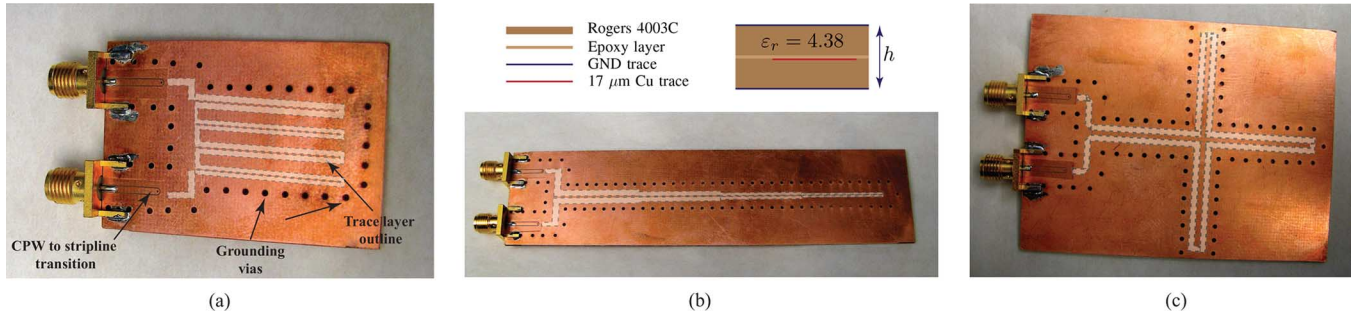
Fig. 4. Photographs of coupled-line phaser prototypes in stripline technology consisting of $N = 4$ coupled-line sections in three different configurations. (a) CCS phaser. (b) CCL phaser. (c) HC coupled-line phaser. The photographs show the grounding vias and outline of the copper traces sandwiched between the two substrate layers. Linewidth and line-gap of each coupled-line section are $\ell_i \in [22\ 22\ 22\ 22]$ mil and $g_i \in [22\ 17\ 12\ 7]$ mil, which corresponds to the coupling coefficients $k_i \in [0.065\ 0.095\ 0.145\ 0.215]$ extracted from full-wave simulation (FEM-HFSS). Length of each section is 1000 mil.

1) While the delay values of the peaks in the CCL case are near identical, except for the 1st and the Nth peak, a strong variation of the delay peak values occurs in the HC case, with the central peak exhibiting the largest group-delay swing.

2) The HC coupled-line phaser provides the largest group-delay swing, and the largest absolute delay values, among the three cases, at the cost of locally reduced bandwidth around the peak values.

3) Compared to the CCL coupled-line phaser, the spacing between adjacent peaks across the bandwidth is strongly nonuniform in the case of HC coupled-line phasers, with more crowding near the center of the periodic bandwidth.

It should be noted that the group-delay response of an HC coupled-line coupler is *not* simply a superposition of the responses to the corresponding CCS and CCL phasers.

Despite the very different group-delay characteristics, the following theorem is common to the three phaser configurations: *Given N sections, the total area under the $\tau - \theta$ curve is $N\pi$ regardless of the configuration.* This theorem is demonstrated in Appendix, Section D. As a result, based on the aforementioned considerations regarding the number of delay peaks, compared to the weakly dispersive CCS phasers, the CCL and HC phasers make a more efficient use of their delay-frequency area by shaping the delay curve so as to produce higher dispersion regions. In other words, they locally enhances the group-delay peaks around specific frequencies by reducing the other peaks so as to keep the total area constant. A detailed wave-interference mechanism will be used in Section III to explain the other delay characteristics of these phaser configurations.

D. Experimental Illustrations

In order to confirm the delay characteristics of the three coupled-line configurations, their prototype were built, in stripline technology, as shown in Fig. 4. The prototypes consist of two RO4003C substrate layers, each 20-mil thick. The stripline is fed through a coplanar-waveguide to stripline transition at each input and output port. An array of conducting vias following the signal layer profile were used to maintain the same potential between the top and ground planes.
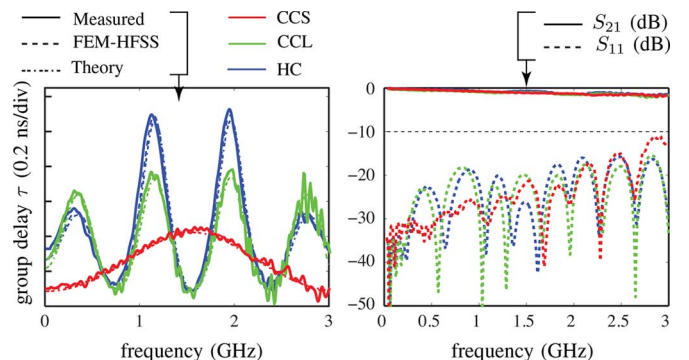

Fig. 5. Measured S-parameters and group-delay responses of the prototypes shown in Fig. 4 compared with full-wave and theoretical results.

Fig. 5 shows the measured S-parameters and the group-delay responses for the three prototypes of Fig. 4, corresponding to the CCS-, CCL-, and HC phasers for $N = 4$. All prototypes are well matched across the entire bandwidth of interest with $S_{11} < -10$ dB in all cases. An excellent agreement between measured results, full-wave, and the analytical results of Section II-B, is observed in all cases. As concluded from Fig. 2(b), HC coupled-line phasers provide the largest group-delay swing among all three configurations. Fig. 6(a) shows another prototype for the HC coupled-line phaser with $N = 9$. Again, measured S-parameters exhibit reasonable agreement within the design bandwidth, as seen in Fig. 6(b), with excellent agreement between the measured and simulated group-delay responses. It should be particularly noted that, despite their simplicity, the analytically derived transfer functions predict the various group-delay characteristics in a convincing manner in all cases with a relative delay error of $<1\%$ and $<5\%$ with simulated and measured responses, respectively. These formulas may thus be deemed appropriate for fast and efficient designs of coupled-line phasers.

III. WAVE-INTERFERENCE EXPLANATION

A. Signal Flow Analysis

The transfer function of a coupled-line coupler terminated with an all-pass transfer function S_0 was derived in the Appendix, Section B using a scattering matrix approach. An alternative approach to obtain such a transfer function is using
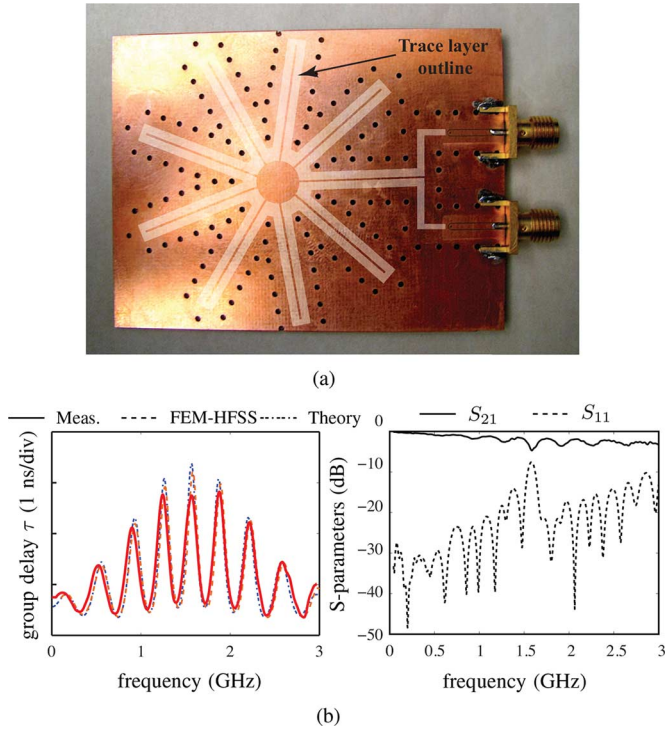
(a)

(b)

Fig. 6. HC coupled-line phaser with $N = 9$ coupled-line sections. (a) Photographs. (b) Measured group-delay response. (c) Measured S-parameters. Linewidth, line-gap, and length of every section are 20, 8, and 1000 mil, respectively.
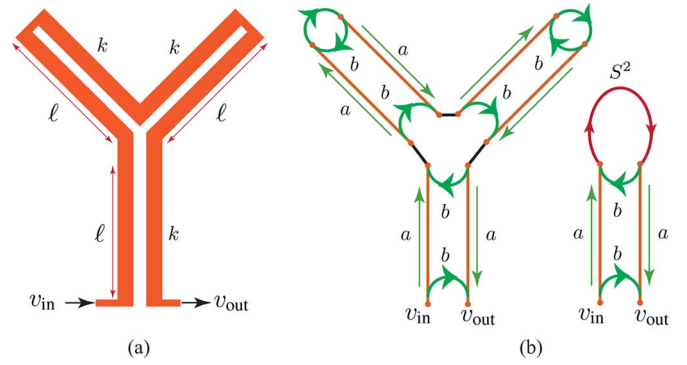

Fig. 7. Wave interference phenomenology in HC coupled-line phasers. (a) Phaser layout for $N = 3$ coupled-line sections of identical lengths and couplings k. (b) Corresponding signal flow graph in terms of the coupled-transfer function b and the through transfer function a. S is the overall transfer function of a single C-section.

the signal flow graph analysis in conjunction with wave interference consideration [31], [32]. The signal flow graph analysis provides deeper insight into the wave propagation mechanisms involved and is thereby instrumental to unveil the group-delay characteristics of coupled-line phasers.

Let us consider an HC coupled-line phaser with $N = 3$, composed of ideally matched coupled-line sections with infinite isolation, as shown in Fig. 7(a). Let us also assume that all coupled sections have the same length and coupling coefficient. Each coupled-line section has frequency dependent through and coupled transfer functions, a and b, respectively [see (12)]. The structure may be seen as a coupled-line coupler terminated with a pair of CCS. The corresponding signal flow graph is shown in Fig. 7(b). In the terminating C-sections, the through signal component is coupled back into the structure via the end connection, resulting in the formation of signal loops, which provides the necessary variation in the delay across the design bandwidth [32]. The problem can be simplified by considering a net transfer function S^2 representing the complete termination, as indicated in Fig. 7(b).

Based on the simplified signal flow of Fig. 7(b), the contributions of the different waves along the structure may be summed up to build the overall transfer function S_{21} as

$$
S_{21}(\theta) = \overbrace{b}^{\text{direct coupled}} + \overbrace{(a \times S^2 \times a)}^{\text{direct through}}
$$
$$
+ \underbrace{(a \times S^2 \times b \times S^2 \times a)}_{\text{first loop}}
$$

$$
\overbrace{+ \, (a \times S^2 \times b \times S^2 \times b \times S^2 \times a)}^{\text{second loop}} + \cdots
$$
$$
= b + a^2 S^2 [1 + bS^2 + b^2 S^4 + b^3 S^6 + \cdots]
$$
$$
= b + \frac{a^2 S^2}{1 - bS^2} \tag{7}
$$

which is identical to (2) obtained using the scattering matrix method with $S_0 = S^2$, where S_0 may represent an arbitrary all-pass function. Since the overall transfer function is all-pass, it may be expressed as $e^{j\phi}$ ($|e^{j\phi}| = 1, \forall \phi$), and (7) may be compactly rewritten as

$$
S_{21}(\theta) = e^{j\phi} = b + a^2 S_0 S_{\text{loop}} \tag{8a}
$$

with

$$
S_{\text{loop}} = \sum_{n=0}^{\infty} b^n S_0^n. \tag{8b}
$$

Differentiating (8a), using the definition $\tau(\omega) = -d\phi/d\omega$, and rearranging the terms yields

$$
\tau(\omega) = je^{-j\phi} \left\{ \overbrace{\frac{db}{d\theta}}^{\text{Term I}} + \overbrace{\frac{a^2}{b}\left(S_0\frac{db}{d\theta} + b\frac{dS_0}{d\theta}\right)\Gamma_{\text{loop}}}^{\text{Term II}} \right.
$$
$$
\left. + \overbrace{S_{\text{loop}}\left(2aS_0\frac{da}{d\theta} + a^2\frac{dS_0}{d\theta}\right)}^{\text{Term III}} \right\} \frac{d\theta}{d\omega} \tag{9a}
$$

with

$$
\Gamma_{\text{loop}} = \sum_{n=0}^{\infty} nb^n S_0^n. \tag{9b}
$$

In the particular case $S_0 = 1$, the HC coupled-line phaser reduces to the single C-section with the group delay [32]

$$
\tau(\omega) = je^{j\phi}\left(\frac{db}{d\theta} + \frac{a^2}{b}\frac{db}{d\theta}\Gamma_{\text{loop}} + 2a\frac{da}{d\theta}S_{\text{loop}}\right)\frac{d\theta}{d\omega}. \tag{10}
$$

Comparing the delay expression (9a) of HC phasers to the group delay (10) of a C-section, it appears that both Term II and Term III have an extra factor proportional to $dS_0/d\theta$ contributing to the delay swing when the termination is dispersive, i.e., $dS_0/d\theta \neq 0$. This reveals that the greatness of the group-delay swings observed in the CCL and HC phasers in Section II are essentially due to the dispersive nature of the terminations. In contrast, in the CCS phaser case, which have regular C-sections with nondispersive terminations, i.e., $S_0 = 1$, the coefficients proportional to $dS_0/d\theta$ in Terms II and III vanish, resulting in smaller delay swings.

It should be noted that, in practice, where loss is never zero, phasers including strongly dispersive terminations may exhibit negative group-delay responses. In an electromagnetic medium, the magnitude and phase responses are interrelated by Kramers–Kronig relations, which are the mathematical representation of causality [33]. Consequently, high dispersion, which is associated with high variations in $\mathrm{Re}\{\varepsilon_r\}$ or $\mathrm{Re}\{\mu_r\}$, implies high loss, i.e., high $\mathrm{Im}\{\varepsilon_r$ or $\mathrm{Im}\{\mu_r\}$; this is the phenomenon occurring near resonance in plasmas and ferromagnetic materials [33], [34]. Furthermore, high loss is a necessary condition for obtaining negative group delay [31]. To illustrate the effect of loss on the delay response of a coupled-lines phaser, we consider in Fig. 1 a simple D-section phaser, which may be seen as a coupled-line section terminated with a dispersive C-section load, with different dielectric losses or coupling coefficients. Fig. 8(a) compares two phasers with identical coupling coefficients, but different dielectric losses, and reveals that increasing loss can turn a positive group delay into a negative one [31]. Fig. 8(b) compares two phasers with identical dielectric loss, but different coefficients, and reveals that increasing coupling can also turn a positive group delay into a negative one; this is consistent with causality since increasing coupling in a coupled-line phaser corresponds to increasing dispersion. This example shows that it is important to carefully consider loss in highly dispersive phasers. Practical phasers are not expected to operate in extreme dispersion regimes such as the negative group-delay regime, which is characterized by prohibitively high loss and narrow bandwidth, severely altering the integrity of the signal. If a phaser cannot exhibit sufficient dispersion, and hence, resolution to meet specifications, then it must be implemented in another technology (e.g., reflection type [17] or phaser placed on dispersive medium [35]).

B. Wave Interference Phenomenology in HC and CCL Phasers

Consider again a coupled-line coupler terminated with load of arbitrary all-pass transfer function and a corresponding signal flow graph of the type shown in Fig. 7(b). Without loss of generality, consider the termination to be S_0 instead of S^2 to represent a general termination. Depending on S_0, the phaser may be either an CCL or an HC coupled-line phaser. Following the signal flow graph, the total group delay, $\tau(\theta)$, is given by (9a), with $S_{\mathrm{loop}} = \sum_0^\infty b^n S_0^n$ and $\Gamma_{\mathrm{loop}} = \sum_0^\infty n b^n S_0^n$.

Since the load transfer function, S_0, is assumed to be all-pass, and in general, dispersive, it may be written as $S_0(\theta) = e^{j\phi_0(\theta)} = e^{-j\int \tau_0 d\theta}$. Two extreme cases may then be distinguished as follows.
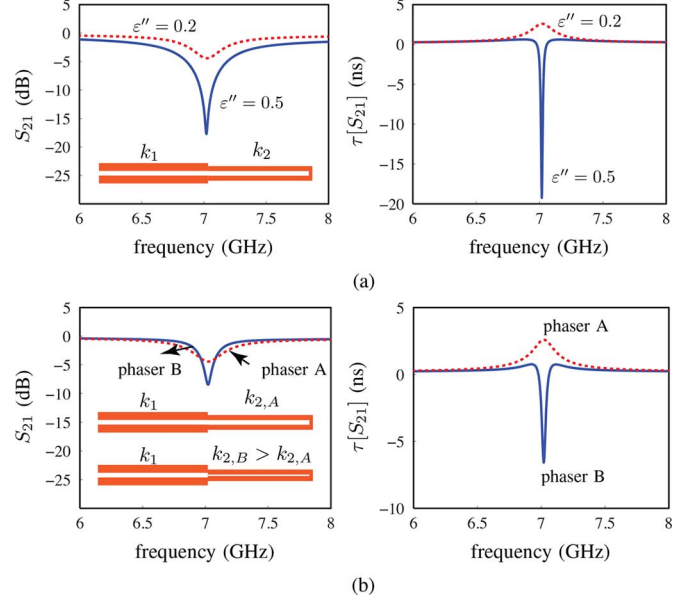

Fig. 8. Effect of loss on the transmission and group-delay responses of a coupled-line phaser (here a D-section with $\varepsilon' = 10.2$). (a) Comparison of two phasers with identical layout (coupling coefficients $k_1 = 0.2$ and $k_2 = 0.99$), but different dielectric losses ($\varepsilon''_A = 0.2$ and $\varepsilon''_B = 0.5$). (b) Comparison of two phasers with identical dielectric loss ($\varepsilon'' = 0.2$), but different coupling coefficients ($k_{2,A} = 0.99$ and $k_{2,B} = 0.999$). Only a small frequency band of interest is shown here.

- *Case I:* if $\phi_0 = 2m\pi$ and $\theta \neq n\pi$ (ensuring $b \neq 0$), where m, n are integers, $S_0 = +1$ so that

$$S_{\mathrm{loop}} = 1 + b + b^2 + b^3 + b^4 + b^5 + b^6 + \cdots$$
$$\Gamma_{\mathrm{loop}} = b + 2b^2 + 3b^3 + 4b^4 + 5b^5 + 6b^6 + \cdots.$$

This represents a *constructive* loop-interference situation where both S_{loop} and Γ_{loop} are maximized, resulting in a *maximum group delay* according to (9a).

- *Case II:* if $\phi_0 = (2m + 1)\pi$ and $\theta \neq n\pi$, where m, n are integers, $S_0 = -1$ so that

$$S_{\mathrm{loop}} = 1 - b + b^2 - b^3 + b^4 - b^5 + b^6 \cdots$$
$$\Gamma_{\mathrm{loop}} = -b + 2b^2 - 3b^3 + 4b^4 - 5b^5 + 6b^6 \cdots.$$

This represents a *destructive* loop-interference situation where both S_{loop} and Γ_{loop} are minimized, resulting in a *minimum group delay* according to (9a).

Let us examine the different types of coupled-line phasers at the light of these observations. First, consider the case of a nondispersive termination, S_0, i.e., a termination with a constant nonzero group delay. Fig. 9(a) shows the typical delay response $\tau[S_{21}]$ of such a phaser. The following two observations can be made.

- The group-delay peaks occur around the regions where the phase of the load ϕ_0 is a multiple of 2π, as expected from Case I above, and vice-versa for the group-delay minima. This is exactly the case for the highest peaks and progressively less from the case for lower peaks.

- The group-delay peaks are uniformly spaced, which is an expected result from the fact that S_0 is nondispersive (linear phase ϕ_0).
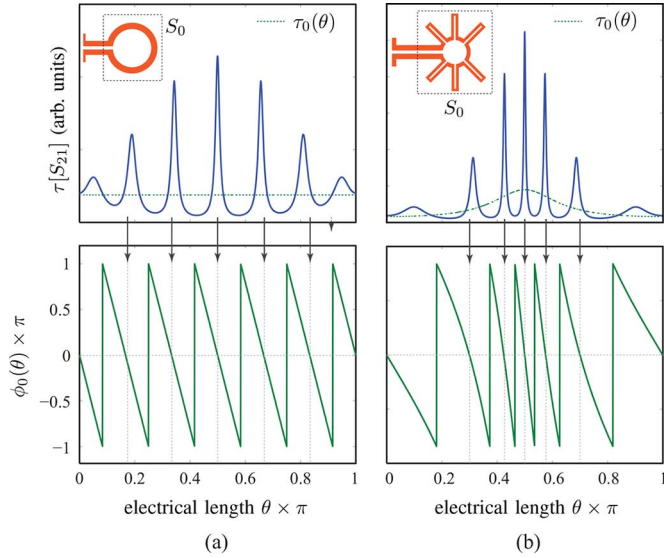
Fig. 9. Typical group-delay response of a coupled-line phaser for the case of: (a) nondispersive and (b) dispersive load, S_0.

Fig. 10. Typical group-delay response of an CCL phaser. (b) Group delay of S_0 in an CCL phaser, compared to that of a regular C-section of equivalent length. (b) Group delay of the CCL phaser related to the transmission phase of S_0. All the lengths are assumed to be equal and $k_i < k_{i+1} \forall i$ in the case of an CCL phaser.

Now consider a dispersive termination S_0 as in an HC coupled-line phaser. Fig. 9(b) shows the typical delay response in such a case. The dispersive characteristics of S_0 manifests itself in the nonconstant nature of the delay $\tau_0(\theta)$ and in the strong wavelength compression region around $\theta = \pi/2$. Again, the locations of the various group-delay peaks of the phaser occur around the regions where the phase of the termination ϕ_0 is $2m\pi$, and vice-versa for the group-delay minima. Furthermore, the adjacent delay peaks are now nonuniformly spaced, with closely packed peaks in the highly dispersive region of S_0. In conclusion, while the locations of $2m\pi$ phase values in ϕ_0 determine the locations of the delay peaks of the phaser, the dispersive nature of the termination S_0 controls the spacing between the adjacent peaks.

Finally, consider an CCL phaser, as illustrated in Fig. 10. In this case, the transfer function of the load of the $i = 0$ coupled-line section is the transfer function of another CCL phaser formed between the first section and the sixth section. Compared to the HC coupled-line phaser, the closed-form expression of S_0 is not readily available, as it must constructed iteratively, as done in the Appendix , Section C. In this situation, a more qualitative approach may be followed to deduce the effects of S_0 in an CCL configuration. The termination function S_0 may be seen as a regular C-section, having a transfer function S_0^C of the same size with *small perturbations* in the coupling coefficients along the structure. Since a conventional C-section has a periodic delay response with uniformly spaced peaks, the CCL phaser must exhibit a similar delay pattern in the small perturbation limit. Fig. 10(a) confirms this prediction, as $\tau_0(\theta)$ closely resembles the delay response of a regular C-section, $\tau_0^C(\theta)$, except at the two extreme ends where the peaks are slightly smaller. Once the termination S_0 is known, the delay response of the overall phaser can be easily found. Fig. 10(b) shows the overall group delay of the phaser, and as described above, the locations of the various group-delay peaks of the phaser occur around the regions where the phase of the termination ϕ_0 is a multiple of 2π. Moreover, since these $2m\pi$ locations of $\phi_0(\theta)$
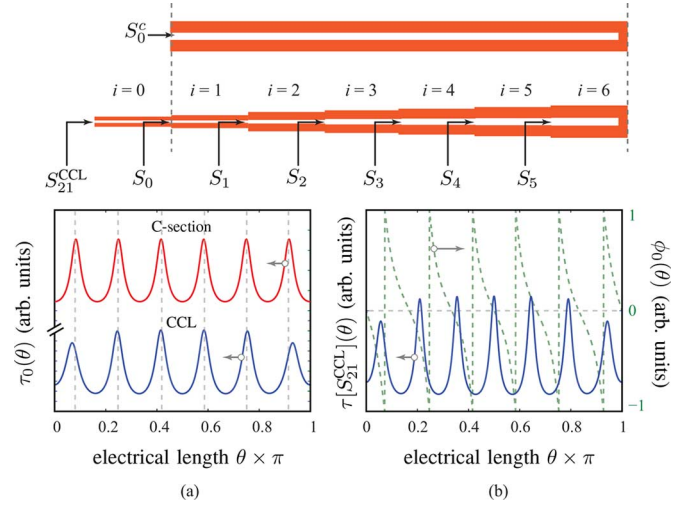
are quasi-uniformly spaced, the resulting delay peaks in $\tau[S_{21}]$ are also quasi-uniformly separated in θ.

The CCL phaser results in Fig. 10 might give the impression that the CCL configuration provides little benefit over a simple C-section since responses shown are very similar. However, the results of Fig. 10 are obtained for coupled-line sections of identical length and small coupling variations, for the sake of the phenomenological explanation. However, if the section lengths are allowed to be different from each other and if the coupling coefficients are allowed to vary more, the CCL configuration may synthesize a great diversity of group delay functions, which is clearly impossible using the single C-section of corresponding length [22].

IV. CONCLUSION

Generalized coupled-line all-pass phasers, based on CCSs, CCLs, and HC coupled transmission line sections, have been presented and demonstrated using analytical, full-wave, and experimental results. The corresponding analytical transfer functions have been derived using matrix methods, which have been found to accurately model the unique group-delay characteristics of these phasers. It has been shown that in contrast to the CCS phaser, CCL and HC coupled-line phasers, consisting of N coupled sections exhibit N group-delay peaks within a harmonic frequency band. Moreover, for a given maximum achievable coupling coefficient, the HC configuration provides the largest group-delay swing, at the expense of reduced bandwidth, around the peak locations. This follows from the fact that the area under the group-delay curve is $N\pi$ regardless the configuration.

Based on the typical group-delay characteristics, it has been shown that the CCS configuration is best suited for broadband phasers, while the CCL and CCS configurations are more suitable for narrowband applications requiring large group-delay swings. A rigorous wave-interference analysis has been applied to the coupled-line phasers so as to provide deep insight into
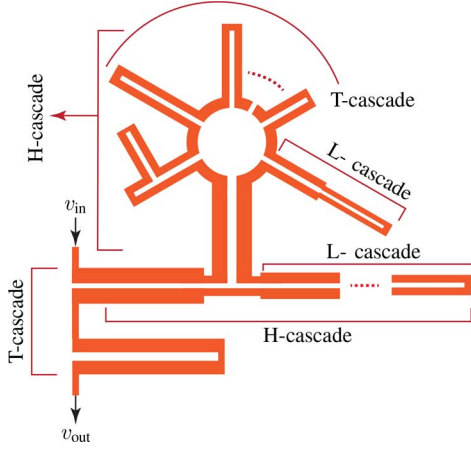
Fig. 11. Generalized coupled-line all-pass phaser consisting of unlimited combinations of CCS, CCL, and HC structures.

the delay mechanisms and the unique group-delay characteristics of CCL and HC coupled-line phasers based on wave propagation phenomenology. The CCS, CCL, and HC configurations represent the three fundamental cascading schemes upon which more complex phasers may be constructed to obtain diverse and rich dispersion characteristics. An illustration of such a construction is shown in Fig. 11, which combines CCS, CCL, and HC topologies into a general coupled-line phaser configuration. Such a configuration enables virtually unlimited group-delay responses, and are anticipated to be useful in synthesizing efficient transmission-line phasers for various R-ASP applications.

APPENDIX

A. Explanation of the Terminology "Phaser"

The terminology "phaser" is meant here to represent electromagnetic signal processors that produce specified frequency sweeping effects in real time [1]. This terminology has been recently used by the authors to designate devices exhibiting diverse and specifiable group-delay (or phase) responses versus frequency, i.e., $\tau = \tau(\omega)$, for various R-ASP applications.[2] However, "phaser" has been used before in acoustics to designate devices producing frequency sweeping effects in real-time (chirping effects) [36], [37] and to designate ferrite phase shifters with typically nonlinear phase-frequency relationships, although the devices were not specifically used for signal processing [38], [39]. Thus, R-ASP phasers referred to herein are devices bearing fundamental commonalities with acoustic- and ferrite-based phasers. Table I places the term "phaser" in global context using comparison with filters, all-pass equalizers, acoustic phasers, and ferrite phasers.

B. Derivation of the C-Section Transfer Function (1a)

Consider an ideal lossless, perfectly matched, and perfectly isolated TEM backward-wave coupled-line coupler, shown in

---

[2]In general, the group-delay function is *nonconstant* (corresponding to a non-linear phase function versus frequency) since group-delay discrimination is necessary for processing. However, one may consider the constant group-delay function as the particular case where the phaser reduces to a simple phase shifter.

TABLE I
CONTEXTUALIZATION OF THE TERMINOLOGY "PHASER" BY COMPARISON
WITH FUNCTIONALITIES AND FEATURES OF OTHER RELEVANT DEVICES

Filters	• Structures or networks *suppressing* electrical or sound waves of unwanted frequencies [40][41]. • *Magnitude engineering* of the transfer function between input port (port 1) and output port (port 2) versus frequency, i.e. $|S_{21}(\omega)| = f(\omega)$, where $f(\cdot)$ is an specified function of frequency ω. • Minimal specification on phase response $\angle S_{21}(\omega) = \phi(\omega)$ although linear phase is most often preferred. • Guided-wave operation where the signal is channeled from the input port to the output port, with *frequency selective surfaces (FSSs)* being its radiative-wave counterpart [42].
All-pass Equalizers	• Structures or networks compensating or *equalizing* phase nonlinearities of the input signal versus frequency [41], [43], [44]. • *Phase engineering* of the transfer function between the input port and the output port versus frequency, i.e. $\angle S_{21}(\omega) = f(\omega)$, where $f(\cdot)$ is a specified function of frequency ω. • Theoretically infinite full transmission bandwidth $|S_{21}(\omega)| = 1$, $\forall \omega$.
Acoustic Phase Shifters or Phasers	• Electronic sound processor filtering an acoustic signal by creating dynamic series of peaks and troughs in the signal's spectrum, so as to produce a *sweeping effect of acoustic frequencies in real-time* [36][37]. • Variation in instantaneous frequency $\omega(t)$ achieved by real-time magnitude engineering. • $|S_{21}(\omega)| \neq 1$ in the operation frequency range.
Ferrite Phase Shifters or Phasers	• Magnetic structures and waveguides achieving *specified phase-shifts* $\angle S_{21}(\omega_0) = \phi_0$ at a given frequency ω_0 [38][39]. • Single frequency design with phase tuning by magnetic bias B_0 [45]. • Desired $|S_{21}(\omega_0) = 1|$ and ideally $\angle S_{21} \neq f(\omega)$ [46].
Electro-magnetic Phase Shifters or Phasers	• Electromagnetic *signal processors* producing specified sweeping effects of frequencies in real time [1], [7], [16], [17], [25], [26], [28]. • Variation in instantaneous frequency $\omega(t)$ achieved by phase/delay engineering. • *Phase/group delay engineering* between the input port and output port versus frequency in a given bandwidth, i.e. $\tau(\omega) = -d\phi(\omega)/d\omega = f(\omega)$ where $\omega \in [\omega_1, \omega_2]$, where $f(\cdot)$ is a specified function of frequency ω. • $|S_{21}(\omega)| = 1$ within $\omega \in [\omega_1, \omega_2]$ [20]. • Generalized term applicable to electromagnetic networks [16][20], structures [23][25] and materials [35] operated either in guided-wave or radiated-wave mode [8], capable of doing signal processing in real-time.

Fig. 12(a). The four-port scattering matrix of such a coupler is [47]

$$\begin{bmatrix} \psi_1^- \\ \psi_2^- \\ \psi_3^- \\ \psi_4^- \end{bmatrix} = \begin{bmatrix} 0 & b(\theta) & a(\theta) & 0 \\ b(\theta) & 0 & 0 & a(\theta) \\ a(\theta) & 0 & 0 & b(\theta) \\ 0 & a(\theta) & b(\theta) & 0 \end{bmatrix} \begin{bmatrix} \psi_1^+ \\ \psi_2^+ \\ \psi_3^+ \\ \psi_4^+ \end{bmatrix} \quad (11)$$

where

$$b(\theta) = \frac{jk \sin \theta}{\sqrt{1-k^2} \cos \theta + j \sin \theta} \quad (12a)$$

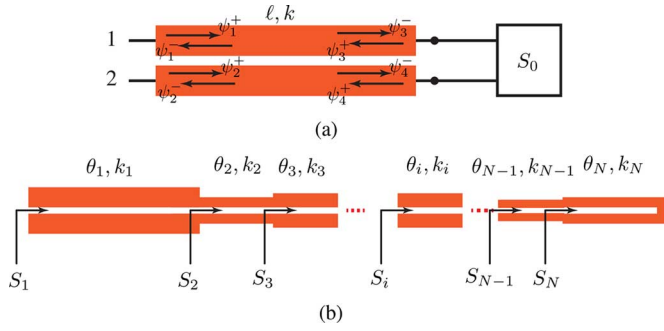$$a(\theta) = \frac{\sqrt{1-k^2}}{\sqrt{1-k^2} \cos \theta + j \sin \theta} \quad (12b)$$

Fig. 12. Coupled-line phaser configurations. (a) C-section terminated with an arbitrary load of transfer function S_0. (b) CCL phaser.

and k is the coupling coefficient. The connection via a two-port of transfer function S_0 of ports 3 and 4 corresponds to the relationship

$$\begin{bmatrix} \psi_3^+ \\ \psi_4^+ \end{bmatrix} = \begin{bmatrix} 0 & S_0 \\ S_0 & 0 \end{bmatrix} \begin{bmatrix} \psi_3^- \\ \psi_4^- \end{bmatrix}. \tag{13}$$

Subsequently prescribing $\psi_3^+ = S_0\psi_4^-$ and $\psi_4^+ = S_0\psi_3^-$ in (13) transforms the four-port coupled-line coupler into a (two-port) C-section described by the following set of equations: $\psi_1^- = b\psi_2^+ + aS_0\psi_4^-$, $\psi_2^- = b\psi_1^+ + bS_0\psi_3^-$, $\psi_3^- = a\psi_1^+/(1 - bS_0)$, and $\psi_4^- = a\psi_2^+/(1 - bS_0)$. These relations lead to the two-port transfer function

$$S_{21}(\theta) = \frac{\psi_1^-}{\psi_2^+} = b + \frac{a^2 S_0}{1 - bS_0}. \tag{14}$$

For $S_0 = 1$, this function may be explicitly written as

$$S_{21}(\theta) = \left(\frac{\sqrt{1+k}\cos\theta - j\sqrt{1-k}\sin\theta}{\sqrt{1+k}\cos\theta - j\sqrt{1-k}\sin\theta} \right)$$
$$= \left(\frac{\rho - j\tan\theta}{\rho + j\tan\theta} \right), \quad \text{where } \rho = \sqrt{\frac{1+k}{1-k}}. \tag{15}$$

C. Derivation of the CCLs Phaser Transfer Function (5)

Consider the CCL sections of Fig. 12(b). The transfer function S_N of the last coupled section is given by

$$S_N(\theta) = \left(\frac{\rho_N - j\tan\theta_N}{\rho_N + j\tan\theta_N} \right) \tag{16}$$

where $\rho_N = \sqrt{1+k_N/1-k_N}$. Using (2), with $S_0 = S_N$, the transfer function of the structure looking into the $(N-1)$th section is found as

$$S_{N-1}(\theta) = b_{N-1} + \frac{a_{N-1}^2 S_N}{1 - b_{N-1}S_N}. \tag{17}$$

Similarly, the transfer function of the structure looking into the $(N-2)$th section can be written in terms of the $(N-1)$th section as

$$S_{N-2}(\theta) = b_{N-2} + \frac{a_{N-2}^2 S_{N-1}}{1 - b_{N-2}S_{N-1}}. \tag{18}$$

Generalizing this procedure, the transfer function of the structure looking into the ith section can be iteratively expressed in terms of the $(i+1)$th section as

$$S_i(\theta) = b_i + \frac{a_i^2 S_{i+1}}{1 - b_i S_{i+1}} \tag{19a}$$

with

$$b_i(\theta) = \left(\frac{jk_i\sin\theta_i}{\sqrt{1-k_i^2}\cos\theta_i + j\sin\theta_i} \right) \tag{19b}$$

and

$$a_i(\theta) = \left(\frac{\sqrt{1-k_i^2}}{\sqrt{1-k_i^2}\cos\theta_i + j\sin\theta_i} \right). \tag{19c}$$

Following this iterative procedure from end to the input of the structure, the overall transfer function of a CCL phaser is found as

$$S_1(\theta) = b_1 + \frac{a_1^2 S_2(\theta)}{1 - b_1 S_2(\theta)}. \tag{20}$$

D. Proof of the Constant Area Under the Group-Delay Curves for CCS, CCL, and HC Phasers

The proof the the area under the group-delay curves for the CCS, CCL, and HC phasers is constant may be conveniently in the low-pass Laplace domain. Consider first the transfer function of C- and D-sections, given by (1a) and (3a), respectively, which become under the high-pass-to-low-pass transformation $s = j\Omega = j\tan\theta$

$$S_{21}^{\text{C-section}}(s) = \left(\frac{\rho - s}{\rho + s} \right) = \frac{H_1(s)}{H_1(-s)} \tag{21a}$$

$$S_{21}^{\text{D-section}}(s) = \left(\frac{\rho_i - s}{\rho_i + s} \right)\left(\frac{\rho_i^* - s}{\rho_i^* + s} \right) = \frac{H_2(s)}{H_2(-s)} \tag{21b}$$

where $H_1(s)$ and $H_2(s)$ are first- and second-order Hurwitz polynomials, respectively, and ρ_i is a function of ρ_a and ρ_b, which are defined in (3).

A general Nth-order all-pass phaser can be expressed in terms of an Nth-order Hurwitz polynomial, $H_N(s) = s^N + c_{N-1}S^{N-1} + \cdots + c_1 s + c_0$, where $c_n \in \Re$, which can always by decomposed as a product of first- and second-order polynomials

$$S_{21}(s) = \frac{H_N(s)}{H_N(-s)} = \prod_{m=1}^{p} \frac{\rho_m - s}{\rho_m + s} \prod_{n=1}^{q} \frac{\rho_n - s}{\rho_n + s}\frac{\rho_n^* - s}{\rho_n^* + s}. \tag{22}$$

This means that any Nth-order all-pass phaser can be realized using p C-sections and q D-sections such that $N = p + 2q$. Consequently, the area under the $\tau - \theta$ curve of a Nth-order all-pass network can be deduced from those of its C- and D-section constituents.

The area under the group-delay curve of an all-pass phaser in a half harmonic period (for symmetry) is

$$I = \int_0^{\pi/2} \tau(\theta)d\theta = \phi(0) - \phi(\pi/2) \tag{23}$$

where the relation $\tau(\theta) = -d\phi(\theta)/d\theta$ has been used. In the Laplace domain, following from $s = j \tan \theta$, the above expression becomes

$$I = \phi_s(0) - \phi_s(j\infty). \tag{24}$$

For a single C-section, corresponding to a first-order polynomial in $s = \alpha + j\sigma$, the phase expression, using (21a), is

$$\phi_s(s) = \tan^{-1}\left(\frac{\sigma}{\alpha - \rho}\right) - \tan^{-1}\left(\frac{\sigma}{\alpha + \rho}\right). \tag{25}$$

Since, subsequently,

$$\phi_s(0) = 0,$$

$$\phi_s(j\infty) = -2 \tan^{-1}\left(\frac{\sigma}{\rho}\right)\bigg|_{\sigma=\infty} = -\pi \tag{26}$$

we have $I = \phi_s(0) - \phi_s(j\infty) = \pi$. Thus, the area under the $\tau - \theta$ curve of a single C-section is π.

Similarly, from (21b), the transmission phase of a single D-section

$$\phi(s) = \tan^{-1}\left(\frac{y - \sigma}{x - \alpha}\right) - \tan^{-1}\left(\frac{y + \sigma}{x - \alpha}\right) \tag{27}$$

$$- \tan^{-1}\left(\frac{y + \sigma}{x + \alpha}\right) + \tan^{-1}\left(\frac{y - \sigma}{x + \alpha}\right) \tag{28}$$

using $\rho = x + jy$. Since

$$\phi_s(0) = 0$$

$$\phi_s(j\infty), = 2\left[\tan^{-1}\left(\frac{y - \infty}{x}\right) - \tan^{-1}\left(\frac{y + \infty}{x}\right)\right]$$

$$= -2\pi \tag{29}$$

we have $I = \phi_s(0) - \phi_s(j\infty) = 2\pi$. Thus, the area under the $\tau - \theta$ curve of a single D-section is 2π.

From (22), the area under the $\tau - \theta$ curve of a general phaser of the Nth order is $p\pi + q(2\pi) = (p + 2q)\pi = N\pi$ with $(p\pi)$ contributed by the p C-sections and $(2q\pi)$ contributed by the q D-sections. Finally, since the transfer function of the CCS, CCL, and HC phaser configurations can be all represented in terms of $H_N(s)$, the area under the $\tau - \theta$ curves is $N\pi$ in a given harmonic period for all three cases.

REFERENCES

[1] C. Caloz, S. Gupta, Q. Zhang, and B. Nikfal, "Analog signal processing," *Microw. Mag.*, vol. 14, no. 6, pp. 87–103, Sep. 2013.
[2] C. Caloz, "Metamaterial dispersion engineering concepts and applications," *Proc. IEEE*, vol. 99, no. 10, pp. 1711–1719, Oct. 2011.
[3] M. Lewis, "SAW and optical signal processing," in *Proc. IEEE Ultrason. Symp.*, Sep. 2005, vol. 24, pp. 800–809.
[4] S. Abielmona, S. Gupta, and C. Caloz, "Compressive receiver using a CRLH-based dispersive delay line for analog signal processing," *IEEE Trans. Microw. Theory Techn.*, vol. 57, no. 11, pp. 2617–2626, Nov. 2009.
[5] H. V. Nguyen and C. Caloz, "Composite right/left-handed delay line pulse position modulation transmitter," *IEEE Microw. Wireless Compon. Lett.*, vol. 18, no. 5, pp. 527–529, Aug. 2008.
[6] B. Nikfal, S. Gupta, and C. Caloz, "Increased group delay slope loop system for enhanced-resolution analog signal processing," *IEEE Trans. Microw. Theory Techn.*, vol. 59, no. 6, pp. 1622–1628, Jun. 2011.
[7] B. Nikfal, D. Badiere, M. Repeta, B. Deforge, S. Gupta, and C. Caloz, "Distortion-less real-time spectrum sniffing based on a stepped group-delay phaser," *IEEE Microw. Wireless Compon. Lett.*, vol. 22, no. 11, pp. 601–603, Oct. 2012.
[8] S. Gupta, S. Abielmona, and C. Caloz, "Microwave analog real-time spectrum analyzer (RTSA) based on the spatial-spectral decomposition property of leaky-wave structures," *IEEE Trans. Microw. Theory Techn.*, vol. 59, no. 12, pp. 2989–2999, Dec. 2009.
[9] J. D. Schwartz, J. Azaña, and D. Plant, "Experimental demonstration of real-time spectrum analysis using dispersive microstrip," *IEEE Microw. Wireless Compon. Lett.*, vol. 16, no. 4, pp. 215–217, Apr. 2006.
[10] M. A. G. Laso, T. Lopetegi, M. J. Erro, D. Benito, M. J. Garde, M. A. Muriel, M. Sorolla, and M. Guglielmi, "Real-time spectrum analysis in microstrip technology," *IEEE Trans. Microw. Theory Techn.*, vol. 51, no. 3, pp. 705–717, Mar. 2003.
[11] B. Xiang, A. Kopa, F. Zhongtao, and A. B. Apsel, "Theoretical analysis and practical considerations for the integrated time-stretching system using dispersive delay line (DDL)," *IEEE Trans. Microw. Theory Techn.*, vol. 60, no. 11, pp. 3449–3457, Nov. 2012.
[12] J. D. Schwartz, I. Arnedo, M. A. G. Laso, T. Lopetegi, J. Azaña, and D. Plant, "An electronic UWB continuously tunable time-delay system with nanosecond delays," *IEEE Microw. Compon. Lett.*, vol. 18, no. 2, pp. 103–105, Jan. 2008.
[13] S. Gupta, B. Nikfal, and C. Caloz, "Chipless RFID system based on group delay engineered dispersive delay structures," *IEEE Antennas Wireless Propag. Lett.*, vol. 10, pp. 1366–1368, Dec. 2011.
[14] M. A. G. Laso, T. Lopetegi, M. J. Erro, D. Benito, M. J. Garde, M. A. Muriel, and M. Sorolla, "Chirped delay lines in microstrip technology," *IEEE Microw. Wireless Compon. Lett.*, vol. 11, no. 12, pp. 486–488, Dec. 2001.
[15] M. Coulombe and C. Caloz, "Reflection-type artificial dielectric substrate microstrip dispersive delay line (DDL) for analog signal processing," *IEEE Trans. Microw. Theory Techn.*, vol. 57, no. 7, pp. 1714–1723, Jul. 2009.
[16] Q. Zhang, S. Gupta, and C. Caloz, "Synthesis of narrow-band reflection-type phaser with arbitrary prescribed group delay," *IEEE Trans. Microw. Theory Techn.*, vol. 60, no. 8, pp. 2394–2402, Aug. 2012.
[17] Q. Zhang and C. Caloz, "Comparison of transmission and reflection all-pass phasers for analog signal processing," *Electron. Lett.*, vol. 49, no. 14, pp. 903–905, Jul. 2013.
[18] C. K. Campbell, *Surface Acoustic Wave Devices and Their Signal Processing Applications*. New York, NY, USA: Academic, 1989.
[19] W. S. Ishak, "Magnetostatic wave technology: A review," *Proc. IEEE*, vol. 76, no. 2, pp. 171–187, Feb. 1988.
[20] Q. Zhang, D. L. Sounas, and C. Caloz, "Synthesis of cross-coupled reduced-order phasers with arbitrary group delay and controlled magnitude," *IEEE Trans. Microw. Theory Techn.*, vol. 61, no. 3, pp. 1043–1052, Mar. 2013.
[21] H.-T. Hsu, H.-W. Yao, K. A. Zaki, and A. E. Atia, "Synthesis of coupled-resonators group-delay equalizers," *IEEE Trans. Microw. Theory Techn.*, vol. 50, no. 8, pp. 1960–1968, Aug. 2002.
[22] E. G. Cristal, "Analysis and exact synthesis of cascaded commensurate transmission-line C-section all-pass networks," *IEEE Trans. Microw. Theory Techn.*, vol. MTT-14, no. 6, pp. 285–291, Jun. 1966.
[23] S. Gupta, A. Parsa, E. Perret, R. V. Snyder, R. J. Wenzel, and C. Caloz, "Group delay engineered non-commensurate transmission line all-passnetwork for analog signal processing," *IEEE Trans. Microw. Theory Techn.*, vol. 58, no. 9, pp. 2392–2407, Sep. 2010.
[24] Y. Horii, S. Gupta, B. Nikfal, and C. Caloz, "Multilayer broadside-coupled dispersive delay structures for analog signal processing," *IEEE Microw. Wireless Compon. Lett.*, vol. 22, no. 1, pp. 1–3, Jan. 2012.
[25] S. Gupta, D. L. Sounas, Q. Zhang, and C. Caloz, "All-pass dispersion synthesis using microwave C-sections," *Int. J. Circuit Theory Appl.*, vol. 42, no. 12, pp. 1228–1245, May 2013.
[26] Q. Zhang, S. Gupta, and C. Caloz, "Synthesis of broadband phasers formed by commensurate C- and D-sections," *Int. J. RF Microw. Comput.-Aided Eng.*, vol. 24, no. 3, pp. 322–331, Aug. 2013.
[27] S. Gupta, L. J. Jiang, and C. Caloz, "Enhanced-resolution folded C-section phaser," in *Int. Electromagn. Adv. Appl. Conf.*, Sep. 2013, pp. 771–773.
[28] T. Paradis, S. Gupta, Q. Zhang, L. J. Jiang, and C. Caloz, "Hybrid-cascade coupled-line phasers for high-resolution radio-analog signal processing," *Microw. Opt. Technol. Lett.*, vol. 56, no. 11, pp. 2502–25 048, Nov. 2014.
[29] W. J. D. Steenaart, "The synthesis of coupled transmission line all-pass networks in cascades of 1 to n," *IEEE Trans. Microw. Theory Techn.*, vol. MTT-11, no. 1, pp. 23–29, Jan. 1963.
[30] E. G. Cristal, "Theory and design of transmission line all-pass equalizers," *IEEE Trans. Microw. Theory Techn.*, vol. MTT-17, no. 1, pp. 28–38, Jan. 1969.

[31] Q. Zhang, D. L. Sounas, S. Gupta, and C. Caloz, "Wave interference explanation of group delay dispersion in resonators," *IEEE Antennas Propag. Mag.*, vol. 55, no. 2, pp. 212–227, May 2013.

[32] S. Gupta, D. L. Sounas, H. V. Nguyen, Q. Zhang, and C. Caloz, "CRLH-CRLH C-section dispersive delay structures with enhanced group delay swing for higher analog signal processing resolution," *IEEE Trans. Microw. Theory Techn.*, vol. 60, no. 12, pp. 3939–3949, Dec. 2012.

[33] J. D. Jackson, *Classical Electrodynamics*, 3rd ed. New York, NY, USA: Wiley, 1998.

[34] L.-P. Carignan, A. Yelon, D. Ménard, and C. Caloz, "Ferromagnetic nanowire metamaterials: Theory and applications," *IEEE Trans. Microw. Theory Techn.*, vol. 59, no. 10, pp. 2568–2586, Oct. 2011.

[35] S. Gupta, L.-P. Carignan, and C. Caloz, "Group delay swing enhancement in transmission-line all-pass networks using coupling and dispersion boosting ferrimagnetic substrate," *Microw. Opt. Technol. Lett.*, vol. 54, no. 3, pp. 589–593, Mar. 2012.

[36] J. O. S. III, *Physical Audio Signal Processing: For Virtual Musical Instruments and Digital Audio Effects*. Stanford, CA, USA: W3K Publishing, 2006.

[37] W. M. Hartmann, "Some psychoacoustical experiments with all-pass networks," *Amer. J. Phys.*, vol. 47, no. 1, pp. 29–34, Jan. 1979.

[38] A. C. Brown, R. Cole, and W. N. Honeyman, "Some applications of ferrites to microwave switches, phasers, and isolators," *Proc. IRE*, vol. 46, no. 4, pp. 722–727, Apr. 1958.

[39] L. R. Whicker and C. R. Boyd, "A new reciprocal phaser for use at millimeter wavelengths," *IEEE Trans. Microw. Theory Techn.*, vol. MTT-19, no. 12, pp. 944–945, Dec. 1971.

[40] "filter, n., v.," in *OED Online*. Oxford, U.K.: Oxford Univ. Press, Sep. 2014.

[41] G. Matthaei, E. M. T. Jones, and L. Young, *Microwave Filters, Impedance-Matching Networks, and Coupling Structures*. Norwood, MA, USA: Artech House, 1980.

[42] B. A. Munk, *Frequency Selective Surface: Theory and Design*. New York, NY, USA: Wiley, 2000.

[43] R. Cameron, C. Kudsia, and R. Mansour, *Microwave Filters for Communication Systems: Fundamentals, Design, and Applications*. New York, NY, USA: Wiley, 2007.

[44] J. Hong and M. Lancaster, *Microstrip Filters for RF/Microwave Applications*. New York, NY, USA: Wiley, 2001.

[45] S. Nakahara, H. Kurebayashi, and A. Mizobuchi, "A 6 GHz rotating field phaser," *IEEE Trans. Magn.*, vol. 8, no. 3, pp. 544–547, Sep. 1972.

[46] C. R. Boyd, L. R. Whicker, and R. W. Jansen, "Study of insertion-phase variation in a class of ferrite phasers," *IEEE Trans. Microw. Theory Techn.*, vol. MTT-18, no. 12, pp. 1084–1089, Dec. 1970.

[47] R. K. Mongia, I. J. Bahl, P. Bhartia, and J. Hong, *RF and Microwave Coupled-Line Circuit*, 2nd ed. Norwood, MA, USA: Artech House, 2007.

Shulabh Gupta (M'09) was born in Etah, India, on December 14, 1982. He received the Bachelors in Technology (B.Tech.) degree in electronic engineering from the Indian School of Mines, Dhanbad, India, in 2004, the Masters of Science (M.S.) degree in telecommunications from the Institut National de la Recherche Scientifique Énergie Matériaux Télécommunications Research Center (INRS-EMT), Université du Quebec, Montréal, QC, Canada, in 2006, and the Ph.D. degree in electrical engineering from the École Polytechnique of Montréal, Montréal, QC, Canada, in 2012. His M.S. thesis research concerned optical signal processing related to the propagation of light in linear and nonlinear optical fibers and fiber Bragg gratings. His Ph.D. research concerned the analog signal-processing techniques using dispersion engineered structures.

From December 2009 to May 2010, he was a Visiting Research Fellow with the Tokyo Institute of Technology, Tokyo, Japan, where he was involved with the application of high-impedance surfaces for oversized slotted waveguide antennas. In 2012, he was a Postdoctoral Fellow with the University of Colorado at Boulder, where he was involved with the design and characterization of high-power ultra-wideband (UWB) antennas. From 2012 to 2014, he was with The University of Hong Kong, as a Post-Doctoral Fellow, where his research concerned multi-functional traveling-wave leaky-wave antennas for RF identification (RFID) and imaging applications. He is currently a Postdoctoral Fellow with the Department of Electrical Engineering, École Polytechnique of Montréal.

Dr. Gupta was a recipient of the Young Scientist Award of EMTS, Ottawa, ON, Canada (2007), URSI-GA, Chicago, IL, USA (2008), and ISAP Jeju, Korea (2011). He was also the recipient of the Best Doctoral Dissertation Award of the École Polytechnique of Montréal (2012), the Prix d'excellence de l'Association des doyens des études supérieures au Québec (ADÉSAQ) Édition (2013) in Québec for his thesis, and the Academic Gold Medal of the Governer General of Canada.

Qingfeng Zhang (GSM'08–M'11) was born in Changzhou, Jiangsu, China, in 1984. He received the B.E. degree from the University of Science and Technology of China (USTC), Hefei, China, in 2007, and the Ph.D. degree from Nanyang Technological University, Singapore, in 2011, both in electrical engineering.

From June 2011 to December 2013, he was with the Poly-Grames Research Center, École Polytechnique de Montréal, Montréal, QC, Canada, as a Postdoctoral Fellow. Since December 2013, he has been with the South University of Science and Technology of China, Shenzhen, China, as an Assistant Professor. His research interests are focused on emerging novel electromagnetics technologies and multidisplininary topics.

Lianfeng Zou (S'13) received the B.E. degree in electrical engineering from the University of Electronic Science and Technology of China (UESTC), Chengdu, China, in 2004, the M.E. degree in electrical engineering from the Chinese Academy of Sciences, Beijing, China, in 2007, and is currently working toward the Ph.D. degree in electrical engineering at the Poly-Grames Research Center, École Polytechnique de Montréal, Montréal, QC, Canada.

From 2007 to 2012, he was with the China Electronics Technology Group Corporation (CETC), where he was an RF Engineer. His research interests include dispersion processing technologies and their applications to real-time radio systems.

Li Jun Jiang (S'01–M'04–SM'13) received the B.S. degree in electrical engineering from the Beijing University of Aeronautics and Astronautics, Beijing, China, in 1993, the M.S. degree from Tsinghua University, Beijing, China, in 1996, and the Ph.D. degree from the University of Illinois at Urbana-Champaign, Urbana, IL, USA, in 2004.

From 1996 to 1999, he was an Application Engineer with the Hewlett-Packard Company. From 2004 to 2009, he was a Postdoctoral Researcher, Research Staff Member, and Senior Engineer with the IBM T. J. Watson Research Center. Since the end of 2009, he has been an Associate Professor with the Department of Electrical and Electronic Engineering, The University of Hong Kong, Hong Kong. From September 2014 to March 2015, he was also a Visiting Scholar with the University of California at Los Angeles (UCLA). His research interests focus on electromagnetics, computational electromagnetics, integrated circuit (IC) signal/power integrity, IC electromagnetic compatibility (EMC)/electromagnetic interference (EMI), antennas, and multi-physics modeling.

Dr. Jiang is an associate editor for the IEEE TRANSACTIONS ON ANTENNAS AND PROPAGATION, an editor for *Progress in Electromagnetics Research*, and an associate guest editor for a Special Issue of the PROCEEDINGS OF IEEE in 2011 2012. He is an IEEE Antennas and Propagation Society (IEEE AP-S) Member, an IEEE Microwave Theory and Techniques Society (IEEE MTT-S) Member, an ACES Member, and a Member of Chinese Computational Electromagnetics Society. He was the Semiconductor Research Cooperation (SRC) Industrial Liaison for several academic projects. Since 2010, he has been a Technical Program Committee (TPC) member of the IEEE Electrical Design for Advanced Packaging and Systems (EDAPS). He was a TPC member of the 2013 IEEE International Conference on Microwave Technology and Computational Electromagnetics (ICMTCE). He was a Scientific Committee member of the 2010 Workshop on Simulation and Modeling of Emerging Electronics (SMEE). He was a special session organizers of IEEE EDAPS, the International Review of

Progress in Applied Computational Electromagnetics (ACES), the Asia–Pacific Radio Science Conference (AP-RASC), the co-organizer of HKU Computational Science and Engineering Workshops in 2010–2012, a TC-9 and TC-10 member of IEEE EMC-S since 2011, the TPC chair of the 7th International Conference on Nanophotonics (ICNP), a TPC member of the 3rd Conference on Advances in Optoelectronics and Micro/Nano Optics (AOM), the co-chair of the International Workshop on Pulsed Electromagnetic Field, Delft, The Netherlands, 2013, the chair of the 14th IEEE Hong Kong AP/MTT Postgraduate Conference, and session chair of many international conferences. He also serves as a reviewer for IEEE TRANSACTIONS on several topics and for other primary electromagnetics and microwave related journals. He was the recipient of the 1998 HP STAR Award, the 2003 IEEE MTT-S Graduate Fellowship Award, the 2004 Y. T. Lo Outstanding Research Award, and the 2008 IBM Research Technical Achievement Award.

Christophe Caloz (S'00–A'00–M'03–SM'06–F'10) received the Diplôme d'Ingénieur en Électricité and Ph.D. degrees from the École Polytechnique Fédérale de Lausanne (EPFL), Lausanne, Switzerland, in 1995 and 2000, respectively.

From 2001 to 2004, he was a Postdoctoral Research Engineer with the Microwave Electronics Laboratory, University of California at Los Angeles (UCLA). In June 2004, he joined the École Polytechnique of Montréal, Montréal,, QC, Canada, where he is currently a Full Professor, the Holder of a Canada Research Chair (CRC), and the Head of the Electromagnetics Research Group. He is currently a Distinguished Adjunct Professor with King Abdulaziz University(KAU), Jeddah, Saudi Arabia. In 2009, he cofounded the company ScisWave, which develops composite right/left-handed (CRLH) smart antenna solutions for WiFi. He has authored or coauthored over 500 technical conference, letter, and journal papers and 12 books and book chapters. He holds several patents. His research studies have generated approximately 12 000 citations. He is a Thomson Reuteurs Highly Cited Researcher. His research interests include all fields of theoretical, computational, and technological electromagnetics with a strong emphasis on emergent and multidisciplinary topics, particularly including metamaterials, nanoelectromagnetics, exotic antenna systems, and real-time radio.

Dr. Caloz is a Member of the Microwave Theory and Techniques Society (MTT-S) Technical Committees MTT-15 (Microwave Field Theory) and MTT-25 (RF Nanotechnology), a speaker of the MTT-15 Speaker Bureau, the chair of Commission D (Electronics and Photonics), Canadian Union de Radio Science Internationale (URSI), and an IEEE MTT-S representative at the IEEE Nanotechnology Council (NTC). Since 2014, he has been an IEEE Distinguished Lecturer for the Antennas and Propagation Society (AP-S). He was the recipient of several awards, including the University of California at Los Angeles (UCLA) Chancellor's Award for Post-doctoral Research (2004), the IEEE MTT-S Outstanding Young Engineer Award (2007), the E. W. R. Steacie Memorial Fellowship (2013), the Prix Urgel-Archambault (2013), and many Best Paper Awards with his students at international conferences.